Lysosome expansion by selective translation of lysosomal transcripts during phagocyte activation

Victoria E. B. Hipolito[1,2], Jacqueline A. Diaz[2], Kristofferson V. Tandoc[3,4], Amra Saric[1], Ivan Toposiviric[3,4,5,6], and Roberto J. Botelho[1,2*]

[1]Graduate Program in Molecular Science and [2]Department of Chemistry and Biology, Ryerson University, Toronto, Ontario, M5B2K3, Canada

[3]Department of Experimental Medicine, McGill University, [4]The Lady Davis Institute, Jewish General Hospital, [5]Gerald Bronfman Department of Oncology and [6]Department of Biochemistry, Montréal, Quebec H3T 1E2, Canada

Running title: Lysosome expansion and translation

*Corresponding author and Lead Contact: rbotelho@ryerson.ca

Keywords

Organelles, lysosomes, biogenesis, phagocytes, innate immunity, antigen, membranes, mTOR, translation

Abbreviations

BMDM: Bone marrow-derived macrophages, BMDC: bone marrow-derived dendritic cells; DCs: dendritic cells; LPS: lipopolysaccharides; LY: Lucifer yellow; PFA: paraformaldehyde; SIM: structured illumination microscopy; 5' TOP: 5' terminal oligopyrimidine; V-ATPase: vacuolar H^+ ATPase pump

Summary

The mechanisms that govern organelle properties to suit the needs of a cell remain poorly defined. Lysosomes degrade cargo from various routes including endocytosis, phagocytosis and autophagy. For phagocytes, lysosomes are a kingpin organelle since they are essential to kill pathogens and process antigens. During phagocyte activation, lysosomes undergo a striking reorganization, changing from dozens of globular structures to a tubular network, in a process that requires the phosphatidylinositol-3-kinase-Akt-mTOR signalling pathway. Here, we show that lysosomes also undergo a rapid expansion in volume and holding capacity during phagocyte activation. Lysosome expansion was paralleled by the induction of lysosomal proteins but this was unexpectedly independent of TFEB and TFE3 transcription factors, known to scale up lysosome biogenesis. Instead, we demonstrate a hitherto unappreciated mechanism of organelle expansion via mTOR-dependent increase in translation of mRNAs encoding key lysosomal proteins including LAMP1 and V-ATPase subunits. Collectively, we identified a mechanism of rapid organelle expansion and remodelling driven by selective enhancement of protein synthesis.

Introduction

Eukaryotic cells compartmentalize a wide-range of biochemical functions within membrane-bound organelles such as the endoplasmic reticulum, peroxisomes and lysosomes. These organelles can exist in disparate morphologies ranging from many individual vesicular organelles, over stacks of flattened membrane sacs, to a continuous membrane reticulum. Despite this complexity, cells must control organelle number, size and activity to meet the needs of their differentiation state. In addition, cells must adapt these organellar properties in response to intrinsic and extrinsic stimuli that alter the metabolic and functional needs of cells (Behnia and Munro, 2005; Chan et al., 2016; Levy and Heald, 2012; Mills and Taghert, 2012; Mullins and Bonifacino, 2001). Yet, how cells determine organellar properties in response to differentiation state and/or changes in their environment remains one of the most outstanding questions in cell biology.

Immune cells like macrophages and dendritic cells are highly plastic inasmuch as they can adopt “resting”, highly inflammatory, and anti-inflammatory states that differ in their gene expression profile, metabolic programming, secretory pathway activity and endolysosomal membrane system (Janssens et al., 2014; Kelly and O’Neill, 2015; Porta et al., 2015; Trombetta et al., 2003). For instance, macrophages appear to better retain fluid-phase material after activation with phorbol esters (Swanson et al., 1987). In comparison, mature dendritic cells abate the degradative capacity of lysosomal system, which is commonly referred to as the MHC-II compartment, to help preserve antigenic peptides for presentation to adaptive immune cells (Delamarre et al., 2005). In yet another example, LPS-activation of macrophages and dendritic cells transforms lysosomes from a collection of dozens of individual globular organelles into a striking tubular network (Mrakovic et al., 2012; Vyas et al., 2007). Lysosome tubulation is linked to retention of pinocytic cargo, exchange of phagosomal cargo, and antigen processing and presentation (Boes et al., 2002; Chow et al., 2002; Mantegazza et al., 2014; Nakamura et al., 2014; Swanson et al., 1987). This reorganization requires downstream TLR4 signals including the phosphatidylinositol 3-kinase-Akt-mTOR axis, which may interface with the lysosomal Rab7 and Arl8b GTPases to control lysosome association with microtubule-motor proteins (Saric et al., 2016; Vyas et al., 2007). These motors then help distort and tubulate

lysosomes on microtubule tracks (Hollenbeck and Swanson, 1990; Li et al., 2016; Mrakovic et al., 2012).

Notwithstanding that this phenomenon has been widely observed, the molecular underpinnings of lysosome tubulation, distinction between lysosome tubules and punctate lysosomes, and function of tubulated lysosomes remain elusive. This is particularly important since lysosomes interface with various pathways by receiving cargo from the endosomal, phagosomal, autophagosomal and biosynthetic pathways (Appelqvist et al., 2013; Luzio et al., 2007; Settembre and Ballabio, 2014). In addition, lysosomes serve as signaling platforms to sense the metabolic and nutrient state of the cell (Jewell et al., 2013; Lim and Zoncu, 2016; Mony et al., 2016). For instance, a protein network involving the V-ATPase, Ragulator and Rag GTPases sense high levels of amino acids within lysosomes to activate mTORC1 on the lysosome surface (Bar-Peled et al., 2012; Efeyan et al., 2012; Martina and Puertollano, 2013; Sancak et al., 2010; Zhang et al., 2014; Zoncu et al., 2011). Active mTORC1 then phosphorylates various downstream targets to stimulate anabolic pathways including S6 kinase and 4E-BP1, which together enhance mRNA translation (Buszczak et al., 2014; Thoreen, 2017). mTORC1 also represses catabolic pathways that release nutrients during starvation by phosphorylating and repressing ULK, an initiator of autophagy, and inhibiting the transcription factor TFEB, which governs expression of lysosomal genes (Ganley et al., 2009; Jung et al., 2009; Roczniak-Ferguson et al., 2012; Settembre et al., 2012). Thus, mTORC1 is inactivated during starvation to initiate autophagy, boost expression of lysosomal genes and augment macromolecular turnover.

Herein, we set out to further understand the mechanisms underlying the reorganization of the endolysosomal system in activated immune cells. We show that the lysosomal volume and retention capacity is augmented in LPS-activated phagocytes relative to their resting counterparts. In addition, we demonstrate that this expansion is rapid and proceeds through mTOR-dependent induction of lysosomal proteins. Strikingly, this rapid lysosome expansion appears to be independent of transcriptional mechanisms such as activation of TFEB and TFE3 and instead depends on selective and enhanced translation of lysosomal protein-encoding mRNAs.

Results

Activation of macrophage and dendritic cells expands the lysosome volume

Activation of macrophages and dendritic cells elicits a remarkable remodelling of lysosome morphology, converting these organelles from dozens of individual puncta into a tubular network (Boes et al., 2002; Chow et al., 2002; Saric et al., 2016; Swanson et al., 1987). Upon careful visual inspection of this tubular network, we speculated that this tubular lysosome network occupied a larger volume than punctate lysosomes in resting cells (Fig. 1a). To test this, we quantified the total lysosome volume in activated and resting cells by employing image volumetric analysis (Long et al., 2012; Walter et al., 2010). We first pre-labelled lysosomes (see methods and materials for functional definition) with a fluorescent fluid-phase marker and then exposed cells to LPS or vehicle-alone for 2 h to induce lysosome remodelling (Fig. 1a). Pre-labelling cells prior to stimulation ensures that lysosomes are equally loaded with the dye in both resting and activated cells. We then employed live-cell spinning disc confocal microscopy to acquire z-stacks and undertake volumetric analysis. Using this methodology, we observed a significant increase in volume occupied by the fluorescent probe in activated RAW macrophages, primary macrophages and dendritic cells relative to their resting counterparts (Fig. 1b). This suggests that activated phagocytes have an expanded total lysosome volume relative to resting cells.

We previously demonstrated that in RAW macrophages, lysosome tubules were more mobile than punctate lysosomes (Mrakovic et al., 2012). Thus, to exclude the possibility that the increase in lysosome volume was due to a trailblazing effect during Z-stack image acquisition of these cells, we sought to estimate lysosome volume in fixed cells. However, typical fixation protocols with 4% PFA causes tubular lysosomes to disintegrate (Fig. S1a, b). To circumvent this issue, we developed a fixation procedure that preserves lysosome tubules in macrophages (Fig. S1a,b). Re-applying volumetric analysis to fixed RAW cells, we still observed a significant increase in lysosome volume in activated cells relative to resting phagocytes (Fig. 1c). Finally, to exclude that the increase in lysosome volume is an artifact of the limit of

resolution of spinning disc confocal microscopy, we employed structured illumination microscopy (SIM) which enables imaging in super-resolution (Gustafsson, 2005). Due to limitations of the available SIM system, we sampled three x-y planes centred at the mid-point of cells and quantified the area occupied by the fluid-phase marker (Fig. S1c). This approach also demonstrated a significant increase in label volume in activated RAW, primary macrophages, and DCs relative to their resting counterparts (Fig. 1d). These data demonstrate that the lysosome volume expands in response to macrophage and dendritic cell stimulation, concurrent with tubulation.

Phagocyte activation increases lysosomal holding capacity

An expanded lysosome volume may as a corollary lead to a boost in the storage capacity of lysosomes. Hence, we assessed whether activated phagocytes have a higher lysosomal holding capacity relative to resting cells by allowing cells to internalize fluorescent pinocytic tracers to saturation. Indeed, both primary and RAW macrophages pre-activated with LPS exhibited a large increase in fluid-phase accumulation relative to their resting counterparts at each time point examined (Fig. 2a, b; Fig. S2a). We also observed that pre-activated primary macrophages displayed faster rates of pinocytic uptake relative to resting macrophages (Fig. 2c). In fact, the rate of pinocytic uptake was augmented within 15 min of LPS exposure as indicated by macrophages concurrently undergoing pinocytosis and stimulation (Fig. 2c). In comparison, we showed that resting and activated primary macrophages did not differ significantly in the rate of depletion of the pinocytic tracer (Fig. 2d), suggesting that exocytosis rates were similar. RAW macrophages exhibited slightly different dynamics in that the rate of uptake was similar between resting and LPS-stimulated cells (Fig. S2b), but the rate of retention was similar when normalized to initial pinocytic load (Fig. S2c). Collectively, these data indicate that activated macrophages have a higher lysosome holding capacity relative to resting macrophages. Lastly, we questioned whether dendritic cells would benefit from an increase in lysosome volume since they were reported to arrest endocytosis after maturation (Barois et al., 2002; Garrett et al., 2000). However, we note that most reports examine dendritic cell function over 16 h post-stimulation and that more recent work shows that mature cells can still endocytose

extracellular cargo (Drutman and Trombetta, 2010; Kobayashi et al., 2013; Platt et al., 2010). Importantly, we show here that dendritic cells retained their pinocytic capacity up to 8 h post-activation, which fits the timeline of lysosome reorganization and expansion identified in this work (Fig. S2d). Thus, rapidly expanding the lysosome volume may help dendritic cells accumulate more pinocytic content including antigenic material. This is consistent with past reports suggesting that tubulation in activated macrophages may aid in retaining fluid phase and that mature dendritic cells continue to engulf extracellular material (Drutman and Trombetta, 2010; Platt et al., 2010; Swanson et al., 1987, 1985).

Activated macrophages express higher levels of lysosomal proteins

Thus far, the data presented here suggest that activated phagocytes rapidly expand their lysosome volume and retention capacity. Though other mechanisms like increased endosomal membrane influx may contribute to this, we postulated that lysosomal biosynthesis may be a significant driver of lysosome expansion during phagocyte activation. To address this hypothesis, we determined the levels of select lysosomal proteins, namely LAMP1, V-ATPase subunits and cathepsin D by Western blotting in resting and activated macrophages. Specifically, we compared resting macrophages to those continuously exposed to LPS for 2 h or 6 h or for 2 h with LPS followed by a 4 h chase with no LPS. In all cases, LPS induced approximately 2-fold induction of LAMP1 and V-ATPase subunit H protein as compared to resting macrophages (Fig. 3a, b). In contrast, cathepsin D levels remained unchanged (Fig. 3a, b), suggesting that LPS exerts differential effect on lysosomal proteins. The increase in LAMP1 and ATP6V1H was blunted by cycloheximide, indicating that *de novo* protein synthesis, rather than lower protein turnover, augments the levels of lysosomal proteins in LPS-treated phagocytes (Fig. 3a, b). Importantly, cycloheximide blunted lysosome tubulation and expansion in macrophages in response to LPS (Fig. 3c, d). Overall, our data support a role for *de novo* protein synthesis in remodelling and expanding the lysosome network during phagocyte activation.

Rapid lysosome expansion is not dependent on TFEB and TFE3

Our results suggest that biosynthesis plays a major role in LPS-induced lysosome expansion in macrophages. Activation of TFEB and TFE3 transcription factors drives expression of lysosomal genes thereby stimulating lysosome function under various stresses including starvation, phagocytosis, protein aggregation and macrophage activation (Gray et al., 2016; Liu et al., 2017; Martina et al., 2014; Pastore et al., 2016; Polito et al., 2014; Raben and Puertollano, 2016; Sardiello et al., 2009; Settembre et al., 2012, 2013). Thus, we next investigated whether the observed rapid lysosome expansion was driven by TFEB- and TFE3-mediated transcriptional upregulation of lysosome genes.

To assess activation of TFEB and TFE3, we quantified nuclear translocation by quantifying the nuclear-to-cytosol ratio of endogenously expressed proteins by immunofluorescence (Gray et al., 2016; Zhang et al., 2016). As expected, resting cells exhibited mostly cytosolic TFEB and TFE3, whereas inhibition of mTOR for 1 h with torin1 caused both proteins to translocate into the nucleus (Fig. 4a, b). Strikingly, while 2 h incubation with LPS rapidly induced lysosome remodelling and expansion, this did not trigger nuclear translocation of TFEB or TFE3 (Fig. 4a, b). In comparison, a prolonged 6 h incubation with LPS initiated nuclear entry of these proteins, especially for TFE3 that was comparable to mTOR suppression (Fig. 4a, b). These results are consistent with observations by Pastore *et al.,* who also observed delayed nuclear entry of these proteins in response to LPS-induced macrophage activation (Pastore et al., 2016). Strikingly, mRNA levels of TFEB and TFE3 target genes (i.e. LAMP1, TRPML1 and two V-ATPase subunits) were not increased even after 6 h of LPS exposure (Fig. 4c), whereas there was massive upregulation of interleukin-6 mRNA (Fig. 4d).

To further exclude the role of TFEB in lysosome expansion during macrophage activation, we measured tubulation and lysosome volume in RAW macrophages deleted for the genes encoding TFEB and/or TFE3 using CRISPR-based technology (Pastore et al., 2016). Deletion of TFEB and TFE3 did not affect LAMP1 protein levels under resting conditions (Fig. S3a, b) nor fluid-phase marker trafficking, as quantified by Mander's coefficient for dextran-containing LAMP1 signal (Fig. S3c,d). Moreover, both resting control and deletion strains of RAW macrophages accumulated similar levels of the dextran probe after 1 h of uptake and 1 h chase (Fig. S3e). Finally, TFEB and TFE3 status in the cell did not exert major influence on

retention of the fluid-phase probe after 2 h of LPS exposure (Fig. S3f). Collectively, these data suggest that TFEB and/or TFE3 have minimal impact on basal lysosome biogenesis, basal pinocytosis and trafficking to lysosomes.

We next examined early remodelling of lysosomes by treating control and TFEB and/or TFE3-deleted RAW cells with LPS for up to 2h. Importantly, all three mutant cell lines exhibited a significant increase in lysosome tubulation after 2 h of LPS treatment relative to resting condition. This increase in lysosome tubulation in cells devoid of TFEB and/or TFE3 was indistinguishable from that observed in control, TFEB and TFE3 proficient cells (Fig. 4e). Remarkably, LPS-induced expansion of the total lysosome volume was comparable between control and TFEB and/or TFE3-deleted cells (Fig. 4f). Together, these results do not support a role for TFEB and/or TFE3-dependent transcription-based program as a driver for the rapid lysosome expansion during macrophage activation.

Rapid lysosome expansion depends on AKT and mTOR activity

Given that the levels of lysosomal proteins, but not corresponding mRNAs were induced by LPS treatment, we next studied the role of mRNA translation in lysosome expansion. Activated macrophages exhibit extensive metabolic reorganization, enhanced protein synthesis, selective translation of mRNAs encoding inflammatory proteins, and activation of unfolded protein response (Graczyk et al., 2015; Janssens et al., 2014; Kelly and O'Neill, 2015; Porta et al., 2015; Schott et al., 2014). Consistently, LPS activates mTORC1 in macrophages, which not only stimulates mRNA translation, but is also necessary for lysosome tubulation (Buszczak et al., 2014; Saric et al., 2016; Thoreen, 2017). Thus, we first tested whether mTOR activity is necessary for enhanced lysosome volume and holding capacity. Indeed, both primary and RAW macrophages exhibited increased phosphorylation of mTORC1 substrates S6K and 4E-BP1 after exposure to LPS, which is blunted by torin1, which acts as active-site mTOR inhibitor (Fig. 5a, b). Moreover, consistent with our previous observations (Saric et al., 2016), lysosome tubulation was suppressed upon inhibition of mTOR or AKT by torin1 and Akti, respectively (Fig. 5c). Importantly, suppression of AKT and mTOR activity abrogated the LPS-induced expansion of the lysosome volume (Fig. 5d). Finally, the increase in the holding capacity for pinocytic fluid

enticed by LPS treatment was blunted by torin1 (Fig. 5e). Collectively, these findings demonstrate that mTOR is stimulated by LPS, whereby mTOR activation is required for lysosome tubulation, expansion and holding capacity.

Lysosome transcripts are selectively targeted for enhanced translation in an mTOR-dependent manner

Given that mTOR is hyperactivated in LPS-exposed phagocytes and its activity is necessary for lysosome expansion, we next tested whether LPS stimulates global protein synthesis in primary macrophages by employing puromycylation assay. LPS enhanced puromycin incorporation as compared to control in a time-dependent manner, which is indicative of elevated protein synthesis (Fig. 6a, b). Torin1 abrogated the LPS-induced increase in puromycylation (Fig. 6a, b). As a positive control, we demonstrated that translation elongation inhibitor cycloheximide abrogated puromycylation (Fig. 6a, b). Altogether, these results demonstrate that LPS bolsters global protein synthesis in primary macrophages.

In addition to regulating global protein synthesis rates, changes in mTOR activity cause selective alterations in translation of specific mRNA subsets (Masvidal et al., 2017). Considering that LPS increased lysosomal protein levels without altering their stability or corresponding mRNA abundance (Fig. 3A and 4C), we next postulated that mTOR stimulates lysosome expansion by inducing translation of mRNAs encoding lysosomal proteins. To test this hypothesis, we employed polysome profiling wherein mRNAs are separated according to the number of the ribosomes they bind by sedimentation through the 5-50% sucrose gradient (Gandin et al., 2014a). Distribution of mRNAs encoding lysosomal proteins across the gradient was measured by RT-qPCR. Due to technical limitations related to the amount of the material required for polysome profiling studies, these experiments were carried out using RAW macrophages. Relative to the control, LPS treatment shifted LAMP1 and V-ATPase subunit H mRNA distribution towards the heavy polysome fractions, which is indicative of increased translational efficiency (Fig. 7a, b, e and f, Sup. Fig. S5). Importantly, although torin1 exerted minimal effect on the distribution of LAMP1 and V-ATPase subunit H mRNAs in control cells (Sup. Fig. S4), it dramatically reduced loading of these transcripts on heavy polysomes in LPS

treated cells (Fig. 7a, b, e and f, Sup. Fig. S5). These findings indicate that LPS induces translation of LAMP1 and V-ATPase subunit H mRNAs via mTOR. Of note, translational regulation of LAMP1 and V-ATPase subunit H is further supported by the results obtained in primary macrophages wherein LPS treatment induced LAMP1 and V-ATPase subunit H protein levels without affecting their mRNA levels or protein stability (Fig. 3A and 4C). In striking comparison, distribution of mRNAs encoding housekeeping proteins β-actin and PPIA remained unchanged upon addition of LPS and/or torin1 (Fig. 7c, d, g, and h, Sup. Fig. S5). β-actin and peptidylpropyl isomerase A (PPIA) are housekeeping proteins which are not affected by LPS exposure (Gordon et al., 2015; Piehler et al., 2010). Collectively, these observations show that translation of mRNA encoding lysosomal proteins is selectively stimulated during macrophage activation by LPS in an mTOR-dependent manner. This puts forward the model whereby mTOR increases lysosome volume and holding capacity during phagocyte activation by selectively bolstering translation of mRNAs encoding lysosomal proteins.

Discussion

Macrophages and dendritic cells are highly plastic inasmuch as they can dramatically alter their metabolic and gene expression profiles to adopt a range of alternative states, which exert both inflammatory and anti-inflammatory functions. While significant attention has been given to how macrophages and DCs alter their metabolism and expression of cytokines, chemokines and other microbicidal agents, dramatically less is understood regarding the mechanisms that underpin endomembrane system changes during their activation (Janssens et al., 2014; Kelly and O'Neill, 2015; Porta et al., 2015; Trombetta et al., 2003). Most notably, changes to the endomembrane system include reduced degradative capacity of endolysosomes to help conserve antigens in dendritic cells, and a dramatic morphological reorganization of the endolysosome system in both cell types, shifting from a large collection of vesicular organelles into a highly tubular network of lysosomes (Boes et al., 2002; Chow et al., 2002; Delamarre et al., 2005). Tubular lysosomes are thought to play roles in pinocytic retention, exchange of phagosomal content within the endolysosomal system, and delivery of MHC-II-peptide for presentation (Boes et al., 2003; Chow et al., 2002; Mantegazza et al., 2014; Saric et al., 2016;

Swanson et al., 1987). Herein, we show that activated phagocytes also rapidly expand the lysosome volume. We provide evidence that this expansion relies on mTOR-dependent increase in protein synthesis including upregulation of the expression of lysosomal genes at the level of translation.

Re-organization and function of the endolysosome system in activated phagocytes

Here, we disclose that activated macrophages and DCs remodel their lysosome system into an expanded tubular network with augmented holding capacity. This conclusion is supported by several observations. First, imaging volumetric analysis revealed that dyes preloaded into lysosomes occupy a greater volume post-LPS activation using both live- and fixed-cell imaging, as well as super-resolution microscopy. Second, there was an increase in the expression level of several lysosomal proteins that was blunted by cycloheximide treatment. Third, activated macrophages could hold a larger amount of fluid-phase relative to resting counterparts. Thus, overall, activated phagocytes not only undertake morphological reorganization of lysosomes but also expand this organelle. The increase in lysosome volume and holding capacity is consistent with work by Swanson *et al.* done in the 1980s showing that phorbol ester-activated macrophages retain fluid-phase more effectively than resting macrophages (Swanson et al., 1987, 1985). While additional functions are likely, it is reasonable to speculate that expansion of the lysosome volume helps accumulate foreign material within these phagocytes. In this context, it is likely that there are two possible scenarios that may be distinct between macrophages and DCs. In macrophages, lysosome expansion may boost the degradation rate of foreign material engulfed by endocytosis or phagocytosis since the primary function of these cells is pathogen clearance and resolution. In contrast, in DCs, the enlarged lysosome space may increase the capacity to accumulate antigenic material. Indeed, while mature DCs are reported to have reduced endocytosis (Barois et al., 2002; Garrett et al., 2000), we show here that DCs exhibit extensive pinocytosis for at least 8 h post-activation, providing an avenue to internalize and accumulate antigenic material. This is consistent with recent reports revealing that DCs are still able to internalize significant amounts of extracellular content (Drutman and Trombetta, 2010; Platt et al., 2010). Subsequently, the heightened accumulation of antigenic

material, possibly coupled to altered biochemistry of lysosomes, may then improve antigen processing and presentation in these cells.

Mechanistic insight into lysosome volume expansion

Phagocyte activation leads to a rapid expansion of lysosome volume within two hours of LPS exposure. This expansion is driven by biosynthesis as indicated by increased levels of lysosomal proteins and by cycloheximide-mediated block of tubulation and volume expansion. Unexpectedly, our data also suggest that rapid expansion of lysosome volume and capacity in response to LPS stimulation is not dependent on transcription changes to lysosome protein-encoding genes since we did not observe induction of corresponding mRNA levels even after 6 h post-LPS activation. Consistent with this, kinetics of TFEB and TFE3 translocation into the nucleus did not parallel initial lysosome enlargement. Lastly, deletion of these transcription factors did not impair tubulation or rapid lysosome expansion. In contrast to transcriptional programs, we observed that mTOR-dependent translational mechanisms play a key role in lysosome expansion. LPS exposure activates mTOR, as indicated by increased phosphorylation of S6K and 4EBP1, and enhanced protein synthesis, whereas its inhibition abrogated LPS-dependent stimulation of tubulation and lysosome expansion. Importantly, we show that LPS selectively increases translational efficiency of mRNAs encoding lysosomal proteins in mTOR-dependent manner. Of note, mRNAs which encode lysosomal proteins appear to be devoid of the classical 5' terminal oligopyrimidine tract (TOP) which renders transcripts mTOR-sensitive(Hsieh et al., 2012; Jefferies et al., 1994; Meyuhas, 2000; Thoreen et al., 2012). Nevertheless, recent studies suggest that significant number of mTOR-sensitive mRNAs are lacking TOP motif (Bilanges et al., 2007; Gandin et al., 2016; Larsson et al., 2012).

Herein, we focused on the role of *de novo* protein synthesis of lysosomal proteins in lysosomal expansion induced by LPS stimulation. In addition to proteins, lipids must be routed to help expand the lysosome population. This may occur through biosynthesis and/or re-routing membrane flow along the endosomal pathway away from recycling endosomes to lysosomes, or reducing membrane consumption in the formation of multi-vesicular bodies by abating

ESCRT function. Future studies are thus warranted to establish the mechanisms underlying lipid accumulation during lysosome expansion.

Overall, we demonstrate that activated phagocytes dramatically reorganize their lysosomal system by expanding and forming a tubular lysosome network. This expands the lysosome holding capacity of phagocytes, augmenting their ability to internalize and retain fluid-phase cargo. We demonstrate that this process is rapid and requires mTOR-dependent increase in translation of lysosomal mRNAs.

Material and Methods

Cell lines and primary cells

Murine RAW macrophage cell lines carrying CRISPR-mediated deletion of TFEB, TFE3 or both were a kind donation from Dr. Rosa Puertollano, NIH, and were previously described(Pastore et al., 2016). These cells and the wild-type RAW264.7 (TIB-71 from ATCC, Manassas, Virginia) were grown in DMEM supplemented with 5% heat-inactivated fetal bovine serum (Wisent, St. Bruno, Canada) at 37°C with 5% CO_2. Bone marrow–derived dendritic cells (BMDCs) and macrophages (BMDMs) were harvested from wild-type 7-9-week-old female C57BL/6J mice (Charles River Canada, Montreal, QC) as previously described with minor modifications (Inaba et al., 1992; Weischenfeldt and Porse, 2008). Briefly, bone marrow was isolated from femurs and tibias through perfusion with phosphate-buffered saline (PBS) using a 25G syringe. Red blood cells were lysed using a hypoosmotic treatment. For BMDCs, cells were plated at 2 × 10^6/well in 4 ml of DMEM supplemented with 10% fetal bovine serum, 55 µM β-mercaptoethanol, 10 ng/ml recombinant mouse granulocyte-macrophage colony-stimulating factor (PeproTech, Rocky Hill, NJ), and penicillin/streptomycin antibiotics (Wisent). Media was changed every 2 days by replacing half of the medium with fresh medium. For BMDMs, cells were plated according to experimental requirements in DMEM supplemented with 10% fetal bovine serum, 20 ng/ml recombinant mouse macrophage colony-stimulating factor (Gibco, Burlington, ON), and penicillin/streptomycin antibiotics. Media was changed every 2 days. Experiments were conducted on days 7–9. All animals were used following institutional ethics requirements.

Rate, retention and accumulation of pinocytic probes

To measure pinocytosis rate or the accumulation of pinocytic cargo, BMDMs and RAW macrophages were pulsed with 1 mg/mL Lucifer yellow (ThermoFisher Scientific, Burlington, ON) for the indicated time with and without LPS, or after 2 h of LPS pre-stimulation. For pinocytic retention, BMDMs and RAW macrophages were maintained in resting conditions or stimulated with LPS for 2 h, followed by a 30-min pulse with 1 mg/ml Lucifer yellow. Cells were then washed 3x with PBS, and fresh medium was added for the indicated chase periods. In all cases, cells were then washed in PBS, fixed with 4% PFA for 15 minutes and washed in PBS. The amount of Lucifer yellow in RAW macrophages was then quantified using LSRFortessa X-20 cell flow cytometer (BD Biosciences, Mississauga, ON) in 10,000 cells per condition per experiment. Flow cytometry analysis was performed using FCS Express 5 (De Novo Software, Los Angeles, CA). For primary macrophages, Lucifer yellow-labelled cells were visualized using ImageXpress Micro Widefield High Content Screening System (Molecular Devices, Sunnyvale, CA) by where 3x4 quadrants per well were acquired, and the level of probe was analysed using MetaXpress 6 (Molecular Devices). To analyze the pinocytic capacity of BMDCs following activation, cells were pre-stimulated with LPS for the indicated periods, followed by co-incubation with 50 µg/mL of fluorescent dextran in the remaining 30 min of the treatment. Cells were then washed 3x with PBS and fixed with 4% PFA for 15 minutes. Afterwards, dextran fluorescence was imaged by confocal microscopy and quantified with Volocity 6.3.0 image analysis software (PerkinElmer, Bolton, ON) by integrating intensity of dextran.

Lysosome labelling and tubulation

For lysosome labeling, cells were pulsed with 50-100 µg/ml Alexa^{546}-conjugated dextran (ThermoFisher) for 0.5-1 h, followed by 3x wash with PBS and incubated with fresh medium for at least 1 h. To induce lysosome remodeling, BMDMs and BMDCs were exposed to 100 ng/mL LPS from *Salmonella enterica* serotype minnesota Re 595 (Sigma-Aldrich, Oakville, ON), while RAW macrophages were incubated with 500 ng/mL for 2 hours (unless otherwise stated). For pharmacological inhibition, cells were pre-incubated for 15-20 minutes with 100 nM torin1

(Tocris Bioscience, Minneapolis, MN), 10 μM cycloheximide (Bio-Shop) or equivalent volume of vehicle. Cells were then imaged live (unless otherwise indicated) in complete medium. Lysosome were scored as tubules if their length was greater than 4 μm.

Immunofluorescence and Fluorescence Microscopy

To fix and preserve lysosome tubules in RAW cells, cells were incubated with 0.45% (v/v) glutaraldehyde and 0.5% PFA (v/v) in PBS for 15 minutes at room temperature. Cells were then washed with PBS 4x, followed by incubation with 1 mg/mL ice-cold sodium borohydride (Sigma-Aldrich) for 5 min 3x to abate unreacted glutaraldehyde and quench its autofluorescence.

To visualize endogenous TFEB and TFE3, cells were fixed using 4% PFA for 15 min following treatment conditions. Cells were then treated with treated with 100 mM glycine in PBS to quench PFA, then in permeabilization buffer (0.2% Triton-X, 2% BSA in PBS) for 10 min and then blocked for 1 h in 2% BSA. Cells were incubated with rabbit anti-TFEB (1:200; Bethyl Laboratories, Montgomery, TX) or rabbit anti-TFE3 (1:500; Sigma-Aldrich) antibodies for 1 h, followed by Dylight-conjugated donkey polyclonal antibodies against rabbit (1:500; Bethyl) for 1 h. Nuclei were counter stained with 0.4 μg/mL of DAPI. For staining LAMP1, dextran-loaded cells were fixed in 0.45% (v/v) glutaraldehyde and 0.5% PFA (v/v) in PBS for 15 minutes at room temperature. Cells were washed with PBS 3x and quenched in 25mM glycine for 15 mins at room temperature. Cells were permeabilized in ice-cold methanol for 3 minutes and blocked in 2% BSA for 1 h. Cells were then incubated in primary rat anti-LAMP1 (1:100; Developmental Studies Hybridoma Bank) and secondary Dylight-conjugated donkey polyclonal antibodies against rat (1:500; Bethyl) for 1 h each. Cells were then mounted on a slide using DAKO mounting medium.

Live-cell imaging was done at 5% CO_2 and 37 °C using environmental control chambers. Live-cell and fixed-cell imaging was done with a Quorum Diskovery spinning disc confocal microscope system equipped with a Leica DMi8 microscope connected to an Andor Zyla 4.2 Megapixel sCMOS or an iXON 897 EMCCD camera, and controlled by Quorum Wave FX powered by MetaMorph software (Quorum Technologies, Guelph, ON). We also used an Olympus IX81 inverted microscope equipped with a Hamamatsu C9100-13 EMCCD camera and

controlled with Volocity 6.3.0 (PerkinElmer). For super-resolution imaging, we employed the Zeiss Elyra PS1 imaging system equipped with an Axio Observer Z1 microscope fitted with the Andor iXon3 885 detector for structure illumination microscopy (SIM) and powered by Zeiss Zen 2012 software (Zeiss Microscopy, Jena, Germany). Super-resolution image acquisition was acquired by grating for 3 rotations and 5 phases. All SIM reconstructed imaging was done using default settings for image reconstruction; to avoid artifact formation, only images with peak/mean ratios above 20 and noise filter less then -4 were accepted. After reconstruction, Volocity 6.3.0 (PerkinElmer) image analysis software was used. All microscopes were equipped with standard filters appropriate to fluorophores employed in this study, optics and stage automation.

Image analysis and volumetrics

The nuclear-to-cytosolic ratio of TFEB and TFE3 was estimated as the ratio of the mean fluorescence intensity in the nucleus over the mean intensity in the cytosol after background correction using ImageJ (v. 1.47 bundled with 64-bit Java). For Lamp1 and dextran colocalization, we used Manders colocalization analysis to measure the degree of dextran colocalizing in LAMP1 structures, using the JACoP plugin in ImageJ after applying background subtraction. For volumetric analysis, we acquired confocal slices over 0.4 µm z-intervals. Due to technical limitations with SIM super-resolution imaging, we sampled the area of fluorescently labeled lysosomes by acquiring 3 confocal slices in the mid-point of the cell, where we quantified the pixel area for each slice and reported an average per cell. We then used Volocity 6.3.0 image analysis software to quantify the average number of fluorescent voxels or pixels within each cell. Due to the variation in lysosomal size from experiment to experiment we normalized the average voxel or pixel count to the corresponding control group. For lysosomal tubulation, we scored cells as positive for lysosome tubules if they displayed more than four lysosomal tubules greater than 4 µm. Image manipulation was done with ImageJ or Adobe Photoshop (Adobe Systems, San Jose, CA), without altering the relative signals within images or how data may be interpreted. All figures were assembled using Adobe Illustrator (Adobe Systems).

Puromycylation and Western blotting

For puromycylation assays, cells were treated with 10 μg/mL of puromycin (Sigma-Aldrich), or an equivalent water volume for the non-puromycin group, for the last 15 min of each treatment. For all western blot analysis, cells were lysed in Laemmli buffer supplemented with 1:100 protease inhibitor cocktail (Sigma-Aldrich) and PhosSTOP protease inhibitor (Roche, Mississauga, ON) following each treatment. Proteins were then separated in a 10% or 15% SDS-PAGE, for high and low molecular weight proteins, respectively. Proteins were transferred to a polyvinylidene difluoride (PVDF) membrane (EMD Millipore, Toronto, ON), and blocked in 5% skim milk or BSA, in Tris-buffered saline buffer with 0.1% Tween 20 (TBST). Membranes were then immunoblotted using the appropriate primary and secondary antibodies prepared in 5% skim milk or BSA in TBST at the indicated dilutions. The primary antibodies used were rabbit anti-cathepsin D, ATP6V1H (GeneTex Inc., Irvine, CA), p70 S6 kinase, phospho^{Thr389}-p70 S6 kinase, 4E-BP1, phospho$^{Thr37/46}$-4E-BP, β-actin, Tata-box binding protein (TBP; Cell Signaling Technologies, Danvers, MA), all at 1:1,000. We also used mouse anti-puromycin clone 12D10 (1:1000, EMD Millipore), rat anti-LAMP1 (1:200; Developmental Studies Hybridoma Bank, Iowa City, IO) and secondary HRP-linked antibodies raised in donkey (1:10,000, Bethyl). Proteins were detected using Clarity enhanced chemiluminescence (Bio-Rad Laboratories, Mississauga, ON) with a ChemiDoc XRS+ or ChemiDoc Touch imaging system (Bio-Rad). Protein quantification was performed using Image Lab software (Bio-Rad), where protein loading was normalized to levels of Tata box binding protein (TBP) or β-actin, and then normalized against the vehicle group.

Quantitative RT-PCR

For RT-qPCR analysis in BMDMs, total RNA was extracted using the GeneJET RNA purification kit (ThermoFisher). Following RNA isolation, equal quantities of mRNA were reverse transcribed with iScript Reverse Transcription Super Mix (Bio-Rad) following manufacturer's guidelines. The subsequent cDNA was amplified for quantitative PCR using the TaqMan Fast Advanced Master Mix (ThermoFisher) with appropriate TaqMan assays. The CFX96 Touch Real-Time PCR

Detection System (Bio-Rad) and CFX Manager Software (Bio-Rad) were used for amplification and analysis. The TaqMan gene expression assays (ThermoFisher) for the reference gene Abt1 (Mm00803824_m1) and for target genes Atp6v1h (Mm00505548_m1), Atp6v1d (Mm00445832_m1), Lamp1 (Mm00495262_m1), Mcoln1 (Mm00522550_m1) and IL-6 (Mm00446190_m1) were done in triplicate. Target gene expression was determined by relative quantification (ΔΔCt method) to Abt1 and the vehicle-treated control sample.

Polysome profiling

Polysome profiling was performed as detailed in Gandin *et al*. (Gandin et al., 2014b). RAW264.7 cells were seeded in a 15-cm Petri dish and treated for 2 h or 6 h with a vehicle (DMSO), 500 ng/mL LPS from *Salmonella enterica* serotype minnesota Re 595, 100 nM torin1 for 2 h only, or the combination of LPS (500 ng/mL) and torin1 (100 nM) whereby cells were pre-treated for 15 minutes with torin1 before stimulation with LPS. Cells were harvested at 80% confluency, washed twice with ice-cold PBS containing 100 µg/mL cycloheximide and then lysed in hypotonic lysis buffer (5 mM Tris HCl, pH 7.5, 2.5 mM $MgCl_2$, 1.5 mM KCl, 100 µg/ml cycloheximide, 2 mM dithiothreitol (DTT), 0.5% Triton, and 0.5% sodium deoxycholate). Optical density values at 260 nm (OD_{260}) were measured in each lysate and 15 OD_{260} were then loaded on 5–50% sucrose gradients generated using Gradient Master (Biocomp, Fredericton, New Brunswick). Ten percent of lysates were saved as input samples for total RNA extraction. Sucrose gradients were subjected to ultracentrifugation (SW41 Ti 11E1698 rotor; Beckman at 260,000 xg for 2 h at 4 °C) and fractionated by displacement using 60% sucrose/0.01% bromophenol blue on an ISCO Foxy fraction collector (35 s for each fraction, or ~ 750 µL per fraction) equipped with an ultraviolet lamp for continuous absorbance monitoring at 254 nm. Fractions were flash-frozen immediately after fractionation and stored at −80 °C. RNA was isolated with Trizol (Thermofisher) as per manufacturer's instruction. All experiments were carried out at least three independent biological replicates (n=3).

Reverse transcription and RT-qPCR were performed with iScript Reverse Transcription Super Mix (Bio-Rad) and TaqMan Fast Advanced Master Mix (ThermoFisher), respectively. All experiments were carried out at least three independent biological replicates (n=3). Analyses

were carried out using relative standard curve method as instructed by the manufacturer. The following TaqMan assays were done using primers described above and in addition to Actb (Mm02619580_g1) and Ppia (Mm02342430_g1).

Acknowledgments

We would like to thank Dr. Rosa Puertollano at the NIH for her kind donation of the CRISPR-deleted RAW strains (*tfeb*$^{-/-}$, *tfe3*$^{-/-}$ and *tfeb*$^{-/-}$ *tfe3*$^{-/}$ cells). We would like to thank Paul Paroutis and Michael Woodside from the Hospital for Sick Children Imaging Facility (Toronto, ON), and Christopher Spring from St. Michael's Hospital Flow Cytometry Facility (Toronto, ON), for their technical advice and expertise. We would like to thank the technical support staff at the Vivarium Facilities at St. Michael's Hospital for assistance in training and mice maintenance. The LAMP1 hybridoma antibody, developed by J.T. August, was obtained from the Developmental Studies Hybridoma Bank, created by the NICHD of the NIH and maintained at The University of Iowa, Department of Biology, Iowa City, IA.

Funding

This project and related work in the lab of R.J.B. was funded by an Operating Grant from the Canadian Institutes of Health Research, the Canada Research Chair Program, an Early Researcher Award from the Government of Ontario, and Ryerson University. V.E.B.H. was supported by Ontario Graduate Scholarships, Canada Graduate Scholarship and Ryerson Graduate Fellowship. J.A.D was funded by the NSERC undergraduate summer research award. I.T. is a Junior 2 Research Scholar of the Fonds de Recherche du Québec – Santé (FRQ-S) and the work in his lab related to this project was supported by Canadian Institutes of Health Research (PJT-148603).

References

Appelqvist, H., Wäster, P., Kågedal, K., and Öllinger, K. (2013). The lysosome: From waste bag to

potential therapeutic target. J. Mol. Cell Biol. *5*, 214–226.

Bar-Peled, L., Schweitzer, L.D., Zoncu, R., and Sabatini, D.M. (2012). Ragulator is a GEF for the rag GTPases that signal amino acid levels to mTORC1. Cell *150*, 1196–1208.

Barois, N., de Saint-Vis, B., Lebecque, S., Geuze, H.J., and Kleijmeer, M.J. (2002). MHC class II compartments in human dendritic cells undergo profound structural changes upon activation. Traffic *3*, 894–905.

Behnia, R., and Munro, S. (2005). Organelle identity and the signposts for membrane traffic. Nature *438*, 597–604.

Bilanges, B., Argonza-Barrett, R., Kolesnichenko, M., Skinner, C., Nair, M., Chen, M., and Stokoe, D. (2007). Tuberous sclerosis complex proteins 1 and 2 control serum-dependent translation in a TOP-dependent and -independent manner. Mol. Cell. Biol. *27*, 5746–5764.

Boes, M., Cerny, J., Massol, R., Op den Brouw, M., Kirchhausen, T., Chen, J., and Ploegh, H.L. (2002). T-cell engagement of dendritic cells rapidly rearranges MHC class II transport. Nature *418*, 983–988.

Boes, M., Bertho, N., Cerny, J., Op den Brouw, M., Kirchhausen, T., and Ploegh, H. (2003). T Cells Induce Extended Class II MHC Compartments in Dendritic Cells in a Toll-Like Receptor-Dependent Manner. J. Immunol. *171*, 4081–4088.

Buszczak, M., Signer, R.A.J., and Morrison, S.J. (2014). Cellular differences in protein synthesis regulate tissue homeostasis. Cell *159*, 242–251.

Chan, Y.-H.M., Reyes, L., Sohail, S.M., Tran, N.K., and Marshall, W.F. (2016). Organelle Size Scaling of the Budding Yeast Vacuole by Relative Growth and Inheritance. Curr. Biol. *26*, 1221–1228.

Chow, A., Toomre, D., Garrett, W., and Mellman, I. (2002). Dendritic cell maturation triggers retrograde MHC class II transport from lysosomes to the plasma membrane. Nature *418*, 988–994.

Delamarre, L., Pack, M., Chang, H., Mellman, I., and Trombetta, E.S. (2005). Differential lysosomal proteolysis in antigen-presenting cells determines antigen fate. Science *307*, 1630–1634.

Drutman, S.B., and Trombetta, E.S. (2010). Dendritic cells continue to capture and present

antigens after maturation in vivo. J. Immunol. *185*, 2140–2146.

Efeyan, A., Zoncu, R., and Sabatini, D.M. (2012). Amino acids and mTORC1: From lysosomes to disease. Trends Mol. Med. *18*, 524–533.

Gandin, V., Sikström, K., Alain, T., Morita, M., McLaughlan, S., Larsson, O., and Topisirovic, I. (2014a). Polysome fractionation and analysis of mammalian translatomes on a genome-wide scale. J. Vis. Exp.

Gandin, V., Sikström, K., Alain, T., Morita, M., McLaughlan, S., Larsson, O., and Topisirovic, I. (2014b). Polysome fractionation and analysis of mammalian translatomes on a genome-wide scale. J. Vis. Exp.

Gandin, V., Masvidal, L., Hulea, L., Gravel, S.P., Cargnello, M., McLaughlan, S., Cai, Y., Balanathan, P., Morita, M., Rajakumar, A., et al. (2016). NanoCAGE reveals 5' UTR features that define specific modes of translation of functionally related MTOR-sensitive mRNAs. Genome Res. *26*, 636–648.

Ganley, I.G., Lam, D.H., Wang, J., Ding, X., Chen, S., and Jiang, X. (2009). ULK1·ATG13·FIP200 complex mediates mTOR signaling and is essential for autophagy. J. Biol. Chem. *284*, 12297–12305.

Garrett, W.S., Chen, L.M., Kroschewski, R., Ebersold, M., Turley, S., Trombetta, S., Galán, J.E., and Mellman, I. (2000). Developmental control of endocytosis in dendritic cells by Cdc42. Cell *102*, 325–334.

Gordon, E.B., Hart, G.T., Tran, T.M., Waisberg, M., Akkaya, M., Skinner, J., Zinöcker, S., Pena, M., Yazew, T., Qi, C.F., et al. (2015). Inhibiting the mammalian target of rapamycin blocks the development of experimental cerebral malaria. MBio *6*, e00725.

Graczyk, D., White, R.J., and Ryan, K.M. (2015). Involvement of RNA Polymerase III in Immune Responses. Mol. Cell. Biol. *35*, 1848–1859.

Gray, M.A., Choy, C.H., Dayam, R.M., Ospina-Escobar, E., Somerville, A., Xiao, X., Ferguson, S.M., and Botelho, R.J. (2016). Phagocytosis Enhances Lysosomal and Bactericidal Properties by Activating the Transcription Factor TFEB. Curr. Biol. *26*, 1955–1964.

Gustafsson, M.G.L. (2005). Nonlinear structured-illumination microscopy: Wide-field fluorescence imaging with theoretically unlimited resolution. Proc. Natl. Acad. Sci. *102*, 13081–

13086.

Hollenbeck, P.J., and Swanson, J.A. (1990). Radial extension of macrophage tubular lysosomes supported by kinesin. Nature *346*, 864–866.

Hsieh, A.C., Liu, Y., Edlind, M.P., Ingolia, N.T., Janes, M.R., Sher, A., Shi, E.Y., Stumpf, C.R., Christensen, C., Bonham, M.J., et al. (2012). The translational landscape of mTOR signalling steers cancer initiation and metastasis. Nature *485*, 55–61.

Inaba, K., Inaba, M., Romani, N., Aya, H., Deguchi, M., Ikehara, S., Muramatsu, S., and Steinman, R.M. (1992). Generation of large numbers of dendritic cells from mouse bone marrow cultures supplemented with granulocyte/macrophage colony-stimulating factor. J. Exp. Med. *176*, 1693–1702.

Janssens, S., Pulendran, B., and Lambrecht, B.N. (2014). Emerging functions of the unfolded protein response in immunity. Nat. Immunol. *15*, 910–919.

Jefferies, H.B., Reinhard, C., Kozma, S.C., and Thomas, G. (1994). Rapamycin selectively represses translation of the "polypyrimidine tract" mRNA family. Proc. Natl. Acad. Sci. U. S. A. *91*, 4441–4445.

Jewell, J.L., Russell, R.C., and Guan, K.-L. (2013). Amino acid signalling upstream of mTOR. Nat. Rev. Mol. Cell Biol. *14*, 133–139.

Jung, C.H., Jun, C.B., Ro, S.-H., Kim, Y.-M., Otto, N.M., Cao, J., Kundu, M., and Kim, D.-H. (2009). ULK-Atg13-FIP200 Complexes Mediate mTOR Signaling to the Autophagy Machinery. Mol. Biol. Cell *20*, 1992–2003.

Kelly, B., and O'Neill, L.A.J. (2015). Metabolic reprogramming in macrophages and dendritic cells in innate immunity. Cell Res. *25*, 771–784.

Kobayashi, T., Tanaka, T., and Toyama-Sorimachi, N. (2013). How do cells optimize luminal environments of endosomes/lysosomes for efficient inflammatory responses. J. Biochem. *154*, 491–499.

Larsson, O., Morita, M., Topisirovic, I., Alain, T., Blouin, M.-J., Pollak, M., and Sonenberg, N. (2012). Distinct perturbation of the translatome by the antidiabetic drug metformin. Proc. Natl. Acad. Sci. U. S. A. *109*, 8977–8982.

Levy, D.L., and Heald, R. (2012). Mechanisms of Intracellular Scaling. Annu. Rev. Cell Dev. Biol.

28, 113–135.

Li, X., Rydzewski, N., Hider, A., Zhang, X., Yang, J., Wang, W., Gao, Q., Cheng, X., and Xu, H. (2016). A molecular mechanism to regulate lysosome motility for lysosome positioning and tubulation. Nat. Cell Biol. *18*, 404–417.

Lim, C.Y., and Zoncu, R. (2016). The lysosome as a command-and-control center for cellular metabolism. J. Cell Biol. *214*, 653–664.

Liu, A.P., Botelho, R.J., and Antonescu, C.N. (2017). The big and intricate dreams of little organelles: Embracing complexity in the study of membrane traffic. Traffic.

Long, F., Zhou, J., and Peng, H. (2012). Visualization and analysis of 3D microscopic images. PLoS Comput. Biol. *8*, e1002519.

Luzio, J.P., Pryor, P.R., and Bright, N.A. (2007). Lysosomes: fusion and function. Nat. Rev. Mol. Cell Biol. *8*, 622–632.

Mantegazza, A.R., Zajac, A.L., Twelvetrees, A., Holzbaur, E.L.F., Amigorena, S., and Marks, M.S. (2014). TLR-dependent phagosome tubulation in dendritic cells promotes phagosome cross-talk to optimize MHC-II antigen presentation. Proc. Natl. Acad. Sci. U. S. A. *111*, 15508–15513.

Martina, J.A., and Puertollano, R. (2013). Rag GTPases mediate amino acid-dependent recruitment of TFEB and MITF to lysosomes. J. Cell Biol. *200*, 475–491.

Martina, J.A., Diab, H.I., Lishu, L., Jeong-A, L., Patange, S., Raben, N., Puertollano, and Rosa (2014). The nutrient-responsive transcription factor TFE3 promotes autophagy, lysosomal biogenesis, and clearance of cellular debris. Sci. Signal. *7*, ra9.

Masvidal, L., Hulea, L., Furic, L., Topisirovic, I., and Larsson, O. (2017). mTOR-sensitive translation: Cleared fog reveals more trees. RNA Biol. 1–7.

Meyuhas, O. (2000). Synthesis of the translational apparatus is regulated at the translational level. Eur. J. Biochem. *267*, 6321–6330.

Mills, J.C., and Taghert, P.H. (2012). Scaling factors: Transcription factors regulating subcellular domains. BioEssays *34*, 10–16.

Mony, V.K., Benjamin, S., and O'Rourke, E.J. (2016). A lysosome-centered view of nutrient homeostasis. Autophagy *12*, 619–631.

Mrakovic, A., Kay, J.G., Furuya, W., Brumell, J.H., and Botelho, R.J. (2012). Rab7 and Arl8

GTPases are Necessary for Lysosome Tubulation in Macrophages. Traffic *13*, 1667–1679.

Mullins, C., and Bonifacino, J.S. (2001). The molecular machinery for lysosome biogenesis. BioEssays *23*, 333–343.

Nakamura, N., Lill, J.R., Phung, Q., Jiang, Z., Bakalarski, C., de Mazière, A., Klumperman, J., Schlatter, M., Delamarre, L., and Mellman, I. (2014). Endosomes are specialized platforms for bacterial sensing and NOD2 signalling. Nature *509*, 240–244.

Pastore, N., Brady, O.A., Diab, H.I., Martina, J.A., Sun, L., Huynh, T., Lim, J.-A.A., Zare, H., Raben, N., Ballabio, A., et al. (2016). TFEB and TFE3 cooperate in the regulation of the innate immune response in activated macrophages. Autophagy *12*, 1240–1258.

Piehler, A.P., Grimholt, R.M., Ovstebo, R., and Berg, J.P. (2010). Gene expression results in lipopolysaccharide-stimulated monocytes depend significantly on the choice of reference genes. BMC Immunol. *11*, 21.

Platt, C.D., Ma, J.K., Chalouni, C., Ebersold, M., Bou-Reslan, H., Carano, R.A.D., Mellman, I., and Delamarre, L. (2010). Mature dendritic cells use endocytic receptors to capture and present antigens. Proc. Natl. Acad. Sci. *107*, 4287–4292.

Polito, V. a, Li, H., Martini-Stoica, H., Wang, B., Yang, L., Xu, Y., Swartzlander, D.B., Palmieri, M., di Ronza, A., Lee, V.M.-Y., et al. (2014). Selective clearance of aberrant tau proteins and rescue of neurotoxicity by transcription factor EB. EMBO Mol. Med. *6*, 1–19.

Porta, C., Riboldi, E., Ippolito, A., and Sica, A. (2015). Molecular and epigenetic basis of macrophage polarized activation. Semin. Immunol. *27*, 237–248.

Raben, N., and Puertollano, R. (2016). TFEB and TFE3: Linking Lysosomes to Cellular Adaptation to Stress. Annu. Rev. Cell Dev. Biol. *32*, 255–278.

Roczniak-Ferguson, A., Petit, C.S., Froehlich, F., Qian, S., Ky, J., Angarola, B., Walther, T.C., and Ferguson, S.M. (2012). The transcription factor TFEB links mTORC1 signaling to transcriptional control of lysosome homeostasis. Sci. Signal. *5*, ra42.

Sancak, Y., Bar-Peled, L., Zoncu, R., Markhard, A.L., Nada, S., and Sabatini, D.M. (2010). Ragulator-rag complex targets mTORC1 to the lysosomal surface and is necessary for its activation by amino acids. Cell *141*, 290–303.

Sardiello, M., Palmieri, M., di Ronza, A., Medina, D.L., Valenza, M., Gennarino, V.A., Di Malta, C.,

Donaudy, F., Embrione, V., Polishchuk, R.S., et al. (2009). A Gene Network Regulating Lysosomal Biogenesis and Function. Science (80-.). *325*, 473–477.

Saric, A., Hipolito, V.E.B., Kay, J.G., Canton, J., Antonescu, C.N., and Botelho, R.J. (2016). mTOR controls lysosome tubulation and antigen presentation in macrophages and dendritic cells. Mol. Biol. Cell *27*, 321–333.

Schott, J., Reitter, S., Philipp, J., Haneke, K., Schäfer, H., and Stoecklin, G. (2014). Translational Regulation of Specific mRNAs Controls Feedback Inhibition and Survival during Macrophage Activation. PLoS Genet. *10*, e1004368.

Settembre, C., and Ballabio, A. (2014). Lysosome: Regulator of lipid degradation pathways. Trends Cell Biol. *24*, 743–750.

Settembre, C., Zoncu, R., Medina, D.L., Vetrini, F., Erdin, S.S., Erdin, S.S., Huynh, T., Ferron, M., Karsenty, G., Vellard, M.C., et al. (2012). A lysosome-to-nucleus signalling mechanism senses and regulates the lysosome via mTOR and TFEB. Eur. Mol. Biol. Organ. J. *31*, 1095–1108.

Settembre, C., Fraldi, A., Medina, D.L., and Ballabio, A. (2013). Signals from the lysosome: a control centre for cellular clearance and energy metabolism. Nat. Rev. Mol. Cell Biol. *14*, 283–296.

Swanson, J., Burke, E., and Silverstein, S.C. (1987). Tubular lysosomes accompany stimulated pinocytosis in macrophages. J. Cell Biol. *104*, 1217–1222.

Swanson, J. a, Yirinec, B.D., and Silverstein, S.C. (1985). Phorbol esters and horseradish peroxidase stimulate pinocytosis and redirect the flow of pinocytosed fluid in macrophages. J. Cell Biol. *100*, 851–859.

Thoreen, C.C. (2017). The molecular basis of mTORC1-regulated translation. Biochem. Soc. Trans. *45*, 213–221.

Thoreen, C.C., Chantranupong, L., Keys, H.R., Wang, T., Gray, N.S., and Sabatini, D.M. (2012). A unifying model for mTORC1-mediated regulation of mRNA translation. Nature *485*, 109–113.

Trombetta, E.S., Ebersold, M., Garrett, W., Pypaert, M., and Mellman, I. (2003). Activation of lysosomal function during dendritic cell maturation. Science (80-.). *299*, 1400–1403.

Vyas, J.M., Kim, Y.-M., Artavanis-Tsakonas, K., Love, J.C., Van der Veen, A.G., and Ploegh, H.L. (2007). Tubulation of class II MHC compartments is microtubule dependent and involves

multiple endolysosomal membrane proteins in primary dendritic cells. J. Immunol. *178*, 7199–7210.

Walter, T., Shattuck, D.W., Baldock, R., Bastin, M.E., Carpenter, A.E., Duce, S., Ellenberg, J., Fraser, A., Hamilton, N., Pieper, S., et al. (2010). Visualization of image data from cells to organisms. Nat. Methods *7*, S26–S41.

Weischenfeldt, J., and Porse, B. (2008). Bone Marrow-Derived Macrophages (BMM): Isolation and Applications. Cold Spring Harb. Protoc. *2008*, pdb.prot5080-prot5080.

Zhang, C.S., Jiang, B., Li, M., Zhu, M., Peng, Y., Zhang, Y.L., Wu, Y.Q., Li, T.Y., Liang, Y., Lu, Z., et al. (2014). The lysosomal v-ATPase-ragulator complex is a common activator for AMPK and mTORC1, acting as a switch between catabolism and anabolism. Cell Metab. *20*, 526–540.

Zhang, X., Cheng, X., Yu, L., Yang, J., Calvo, R., Patnaik, S., Hu, X., Gao, Q., Yang, M., Lawas, M., et al. (2016). MCOLN1 is a ROS sensor in lysosomes that regulates autophagy. Nat. Commun. *7*, 12109.

Zoncu, R., Bar-Peled, L., Efeyan, A., Wang, S., Sancak, Y., and Sabatini, D.M. (2011). mTORC1 senses lysosomal amino acids through an inside-out mechanism that requires the vacuolar H+-ATPase. Science (80-.). *334*, 678–683.

Figure Legends

Figure 1: LPS-mediated activation of phagocytes augments lysosome volume. a. Lysosomes in bone-marrow derived macrophages (BMDM), bone-marrow derived dendritic cells (BMDCs), and in RAW macrophages before and after 2 h of LPS stimulation, the latter causing extensive lysosome tubulation. Images were acquired by live-cell spinning disc confocal microscopy. Scale bar = 5 µm. **b.** Relative lysosome volume between counterpart resting and LPS-treated phagocytes acquired by live-cell spinning disc confocal imaging. **c.** Relative lysosome volume in fixed resting and LPS-treated RAW macrophages. **d.** Relative lysosome area from the mid-section of resting and LPS-activated phagocytes using images acquired by SIM-enacted super-resolution microscopy. All experiments were repeated at least three independent times. Data

are based on 30-40 cells per condition per experiment and are shown as the mean ± standard error of the mean. Statistical analysis was done using one-way ANOVA and unpaired Student's t-test, where the asterisk * indicates a significant increase in lysosome volume relative to resting phagocytes ($p<0.05$).

Figure 2: Macrophage activation increases lysosomal holding capacity. **a.** Image compilation of 6 representative fields in false-colour showing changes in intensity of Lucifer yellow acquired by endocytosis over the indicated time in resting primary macrophages or macrophages pre-stimulated with 2 h of LPS. Scale 250= µm. Color scale: 0 – 4095 (low-high). **b**. Accumulation of Lucifer yellow continuously endocytosed over indicated timeframe in resting, pre-activated (2 h LPS) or co-activated with LPS. **c**. Rate of pinocytosis of Lucifer yellow in primary macrophages treated as indicated. **d**. Retention of Lucifer yellow in resting or LPS-treated primary macrophages after 0.5 h internalization and chase in probe-free medium over indicate times. In all cases, fluorescence measurements were acquired by fluorimeter plate-imager. Data are shown as the mean ± standard error of the mean from at least 3 independent experiments. Statistical analysis was done using an Analysis of Covariance, whereby controlling for time as a continuous variable. An asterisk indicates a significant increase in Lucifer yellow for that series relative to resting phagocytes ($p<0.05$).

Figure 3: Lysosome remodelling requires protein biosynthesis. **a**. Western blot analysis of whole cell lysates from resting primary macrophages or macrophages exposed to the indicated combinations and time of exposure to LPS and cycloheximide (CHX). **b**. Quantification of Western blots showing the levels of LAMP1, cathepsin D (CtsD) and the V-ATPase V_1 subunit H normalized to TBP. Data are shown as the mean ± standard error of the mean from at least 3 independent experiments. For A and B, "2/4" indicates cells stimulated with 2 h of LPS, followed by a 4 h chase, whereas 2 and 6 h represent cells continuously exposed to LPS for those time periods. **c.** Live-cell spinning disc confocal micrographs of pre-labelled lysosomes in resting primary macrophages resting or those stimulated with LPS and/or cycloheximide. Scale bar = 5 µm. **d.** Relative lysosome volume between resting primary macrophages and those

exposed to specified conditions. Shown is the mean ± standard error of the mean from 30-40 cells for each condition and experiment, across at least 3 independent experiments. Statistical analysis was done with ANOVA and unpaired Student's t-test. The asterisk * indicates a significant difference ($p<0.05$).

Figure 4: Lysosome remodelling is independent of TFEB and TFE3 activation. a. TFEB and TFE3 subcellular localization in resting primary macrophages (vehicle) or those treated with LPS for 2 or 6 h, or with torin1. Green = TFEB or TFE3 immunofluorescence signal; white = nuclei stained with DAPI. Areas within dashed boxes are magnified as insets. **b**. Nuclear to cytosolic ratio of TFEB or TFE3 fluorescence intensity. Shown is the mean ± standard error of the mean from 30-40 cells per condition per experiment across at least 3 independent experiments. **c, d**. Relative mRNA levels of select lysosomal genes (c) or interleukin-6 (d) in activated primary macrophages relative to Abt1 housekeeping gene and normalized against resting cells. Quantification was done by qRT-PCR by measuring the $\Delta\Delta$Ct as described in methods. Shown is the mean ± standard error of the mean from four independent experiments. **e.** Lysosomes in wild-type, *tfeb*$^{-/-}$, *tfe3*$^{-/-}$ and *tfeb*$^{-/-}$ *tfe3*$^{-/-}$ RAW strains before and after 2 h of LPS stimulation. Images were acquired by live-cell spinning disc confocal microscopy. Yellow arrowheads illustrate tubular lysosomes. **f.** Relative lysosome volume between LPS-treated and resting counterpart RAW strains acquired by live-cell spinning disc confocal imaging. Shown is the mean ± standard error of the mean from 30-40 cells per condition per experiment across three independent experiments. All statistical analysis was done with ANOVA and unpaired Student's t-test. The asterisk * indicates a significant difference relative to resting condition ($p<0.05$). For a and e, scale bar = 5 µm.

Figure 5: mTOR stimulates lysosome volume and holding capacity. a. Western blot analysis of whole cell lysates from resting and activated primary macrophages. Total levels and phosphorylation status of S6K and 4EBP1 were monitored using indicated antibodies. TBP served as a loading control. **b.** Normalized ratio of p-p70S6K and p-4EBP1 to total p70S6K and 4E-BP1 protein. Shown is the mean ± standard deviation from three independent blots. **c.**

Lysosomes in primary macrophages were pre-treated with a vehicle (DMSO), Akti or torin1, followed by 2 h LPS stimulation where indicated. Images were acquired by live-cell spinning disc confocal microscopy. Scale bar = 5 µm. **d.** Lysosome volume in primary macrophages treated as indicated normalized to resting macrophages. Shown is the mean ± standard error of the mean from 30-40 cells per condition per experiment across three independent experiments. **e.** Quantification of pinocytic capacity in macrophages treated as indicated. Shown is the mean ± standard error of the mean from four independent experiments. For b and d, data was statistically analysed with ANOVA and unpaired Student's t-test (*p<0.05). For E, data was statistically assessed using an Analysis of Covariance, whereby controlling for time as a continuous variable. An asterisk indicates a significant increase in Lucifer yellow for that series relative to resting phagocytes (*p<0.05).

Figure 6: LPS stimulates global protein synthesis in primary macrophages. a. Western blot analysis of protein puromycylation in resting and activated primary macrophages. LPS increases the amount of puromycylation indicating a boost in global protein synthesis that is blocked by mTOR inhibitors or cycloheximide. Lane 1 are control lysates from cells not exposed to puromycin. The band indicated by arrow is a non-specific band recognized by the anti-puromycin antibody. p-p70S6K and β-actin were used to monitor mTOR status and as a loading control, respectively. **b.** Normalized puromycylation signal (excluding non-specific band) normalized over β-actin signal. Data is shown as the mean ± standard deviation from four independent experiments. Statistical analysis was done with an ANOVA, where * indicates conditions that are statistically distinct from control (*p<0.05).

Figure 7: LPS increases translation of mRNAs encoding lysosomal proteins in an mTOR-dependent manner. a-d. Percent of target mRNA (A: LAMP1, B: ATP6V1H, C: PPIA, and D: β-actin) associated with each ribosome fraction in resting, LPS- or LPS/torin1-treated RAW cells. Left and right panels show 2 h and 6 h treatments, respectively. Shown is a representative experiment (as the mean percentage ± standard error) from four independent experiments,

each of which contained three technical replicates. **e-h:** Pooled percent mRNA in subpolysomal (fractions 7-10), light polysosome (fractions 11 and 12) and heavy polysomes (fractions 13-16). Shown is the mean percent ± standard deviation from four independent experiments with each point in triplicate for each experiment and mRNA. Heavy fractions were statistically analysed by ANOVA and Tukey's post-hoc test, where * indicates statistical difference from resting conditions, while ** indicates differences between LPS and LPS+torin1 conditions within 2 and 6 h exposure.

Figure 1

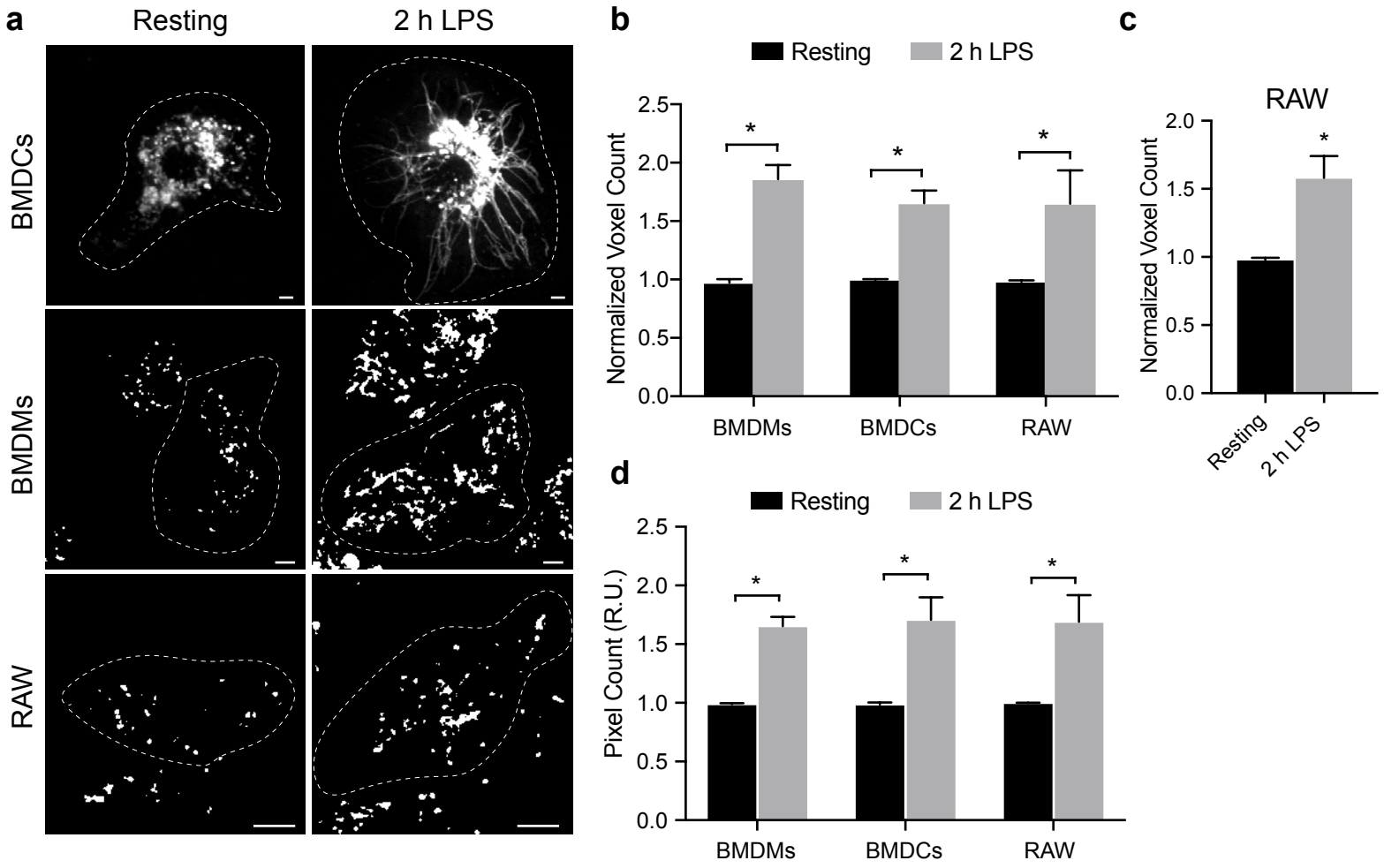

Figure 2

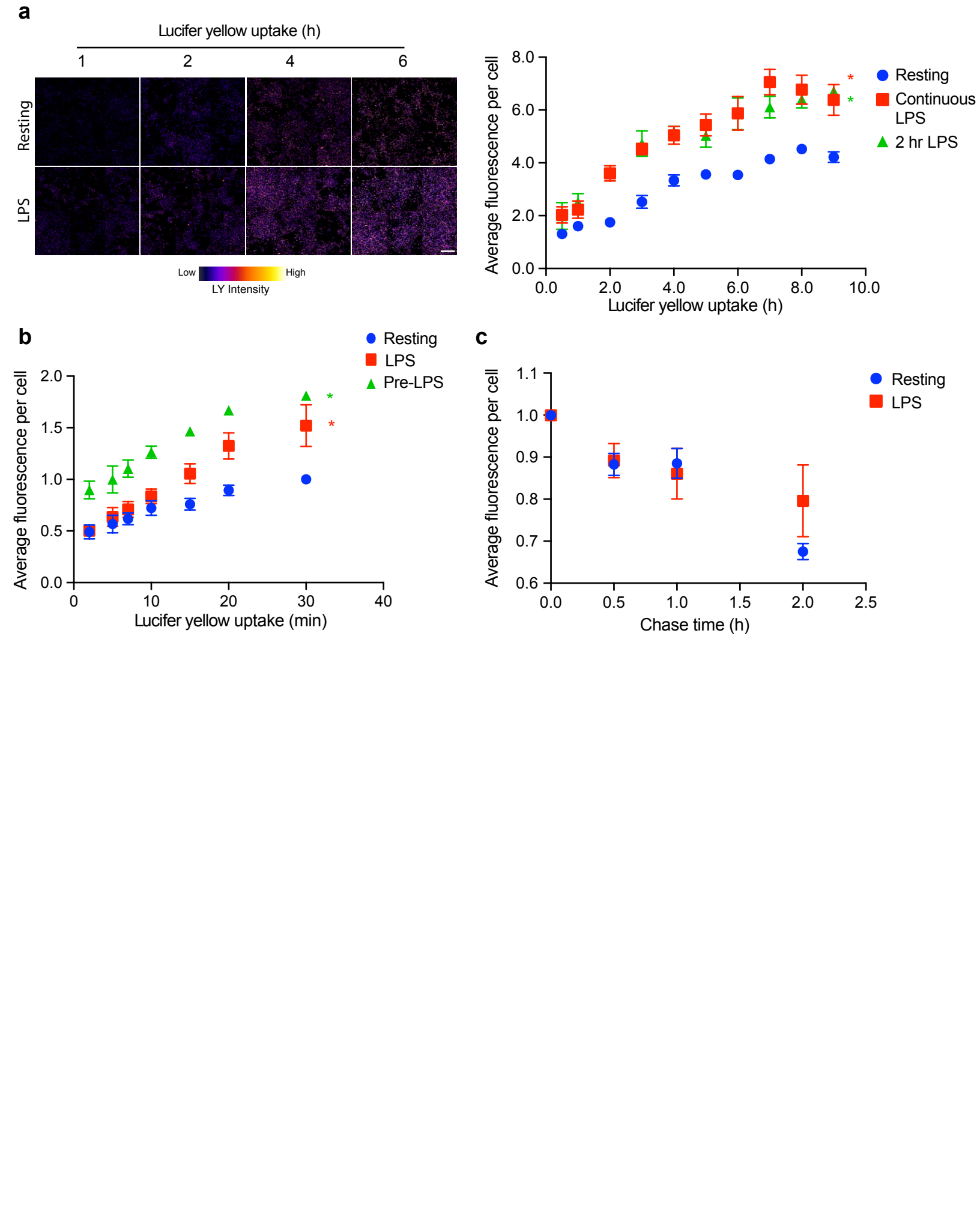

Figure 3

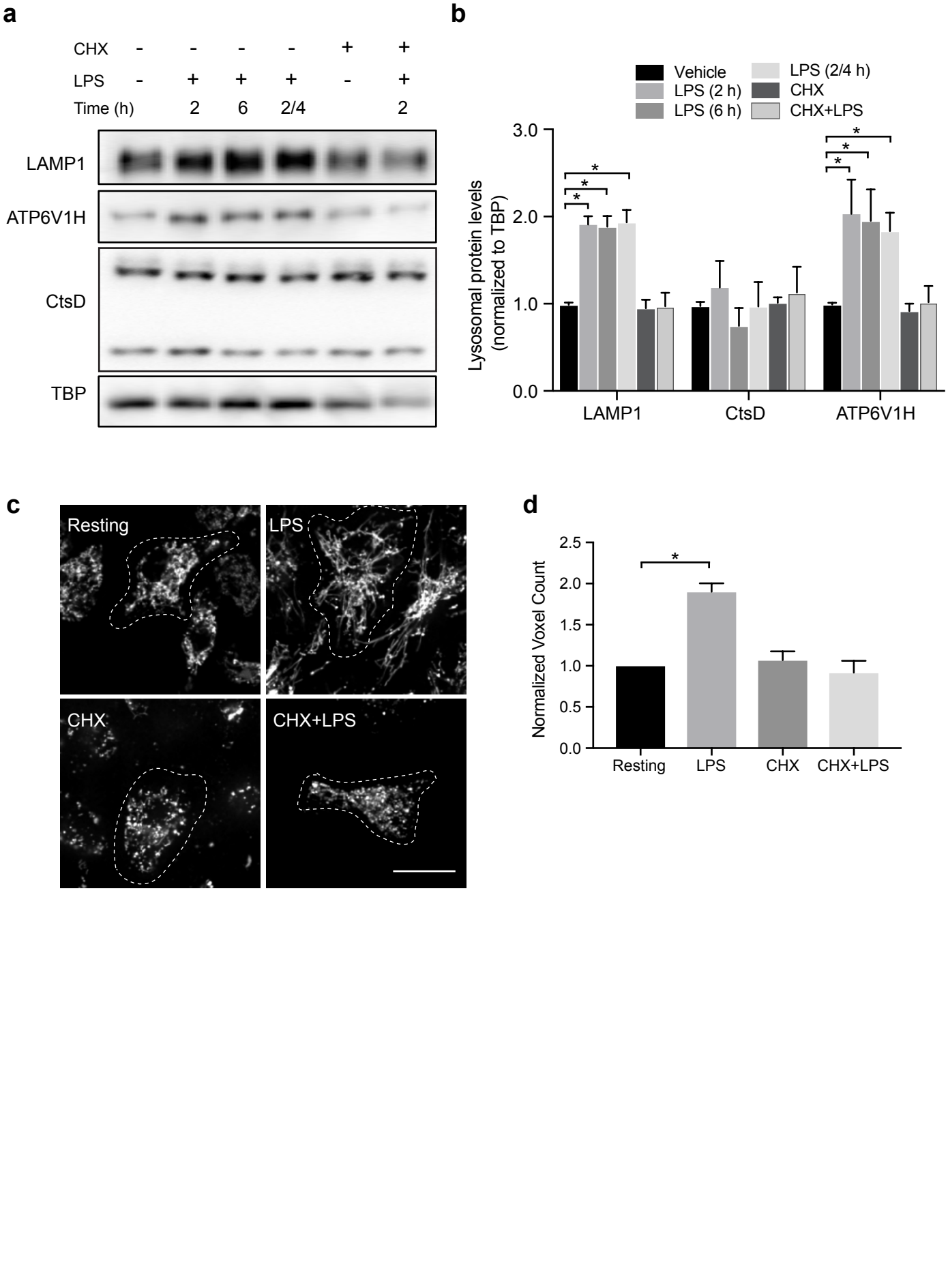

Figure 4

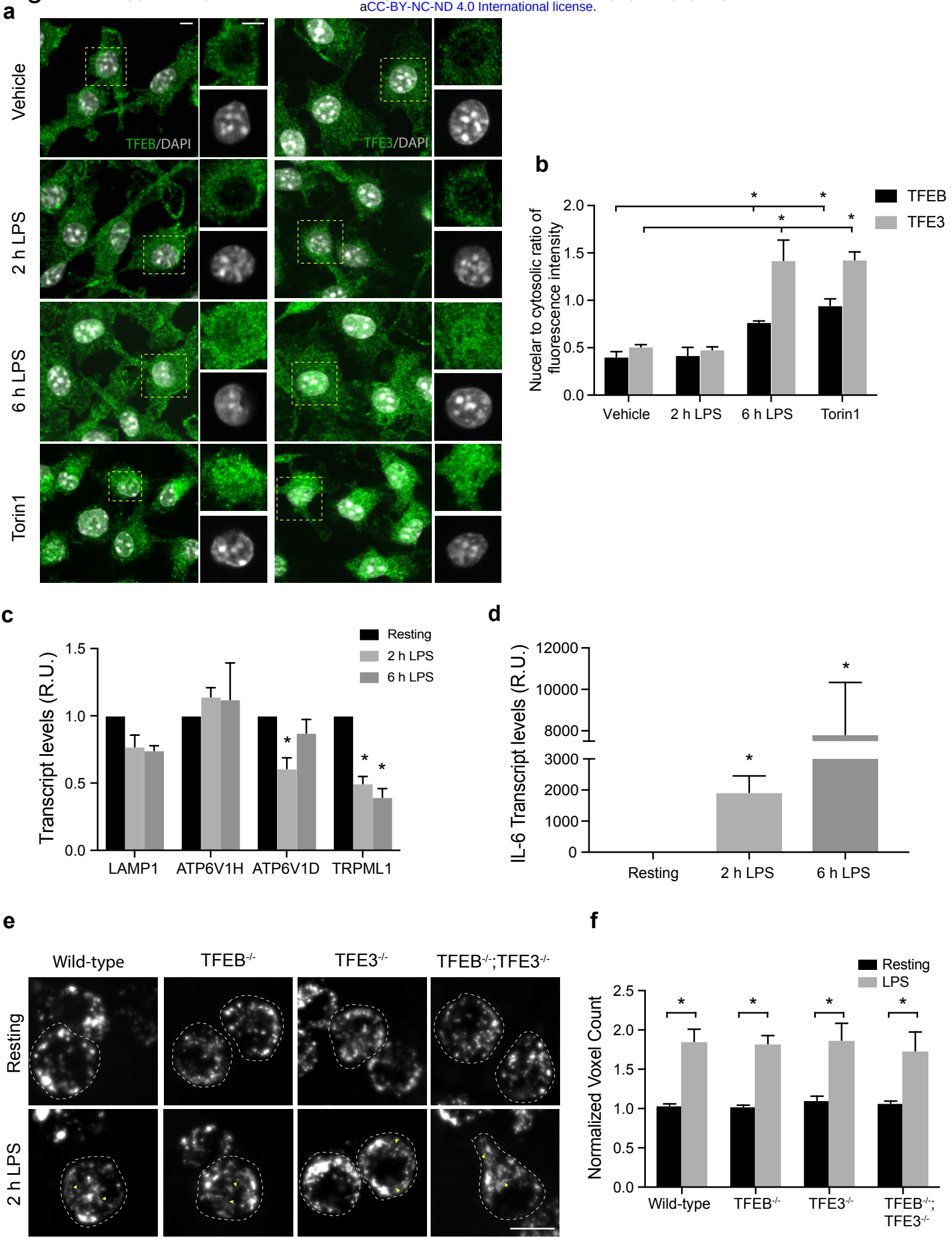

Figure 5

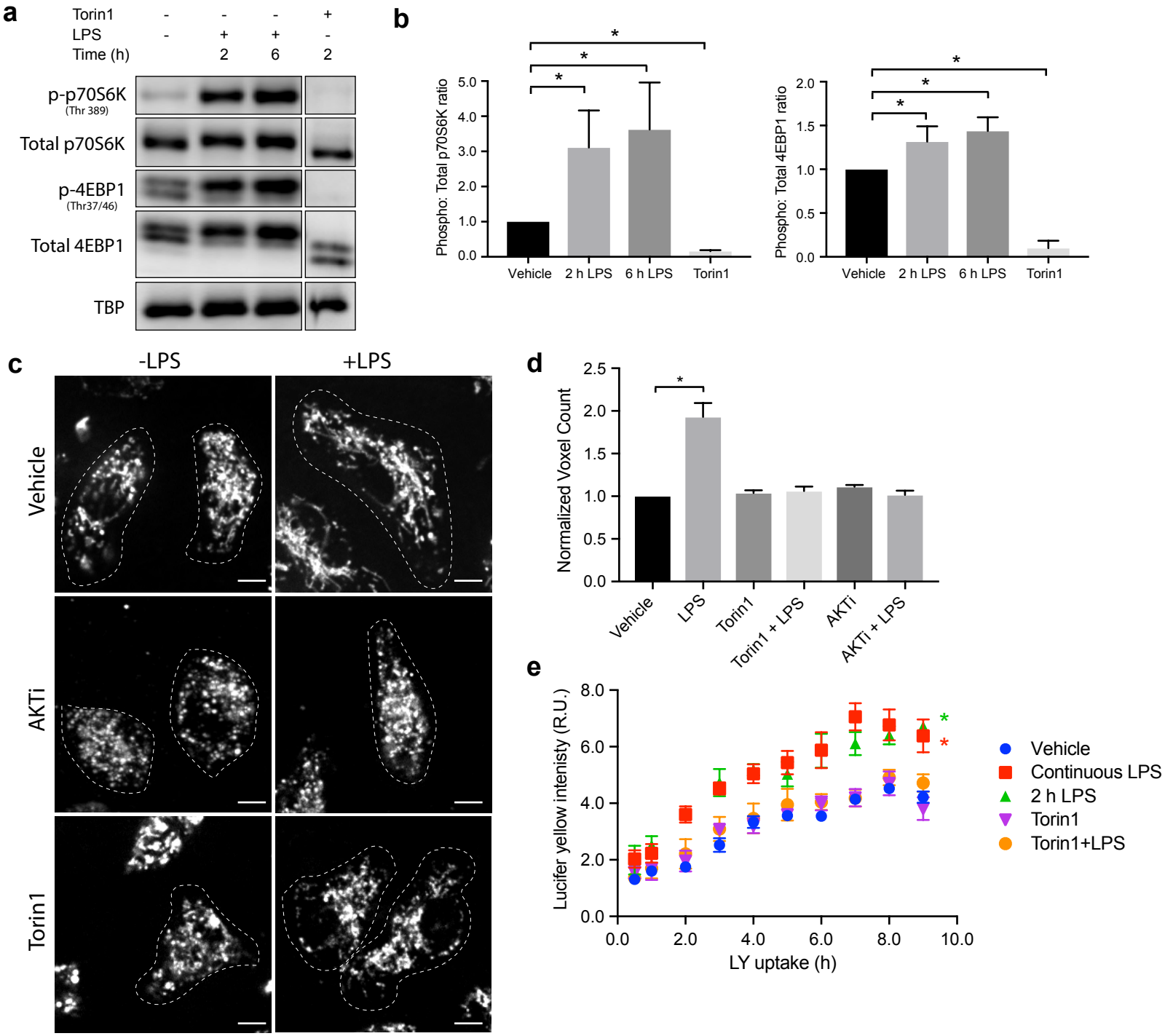

Figure 6

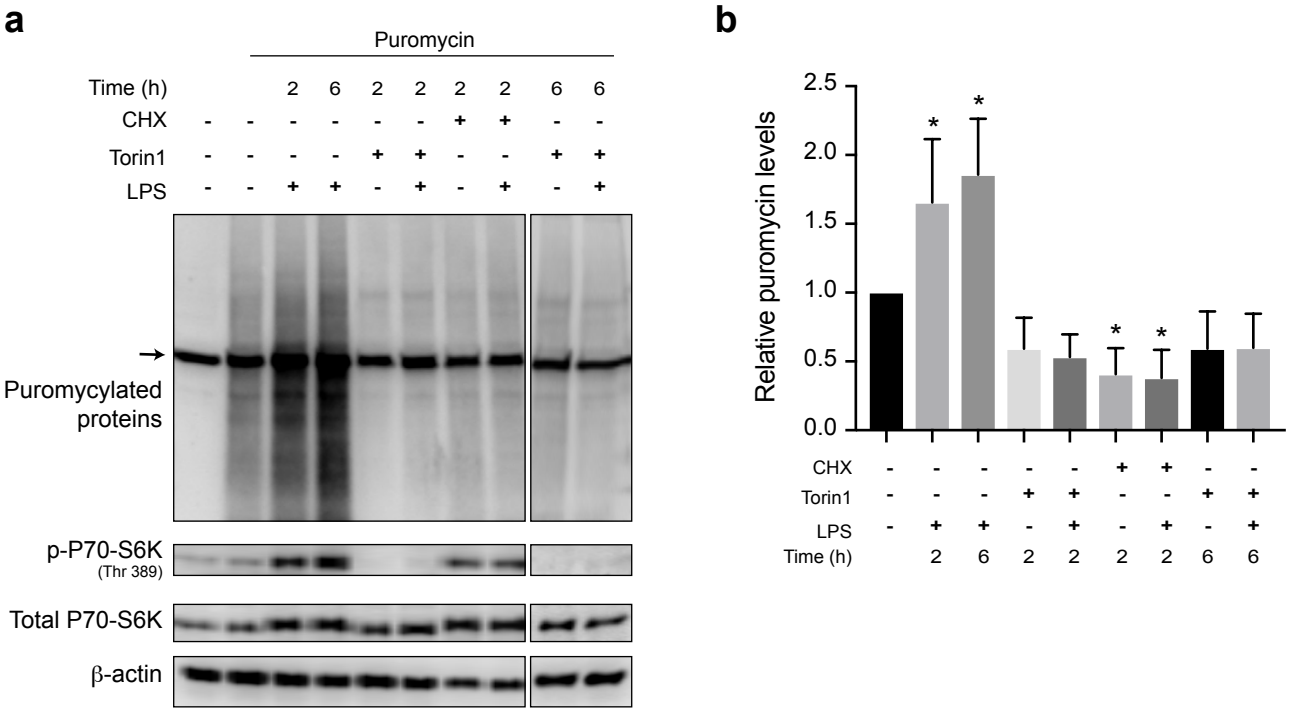

Figure 7